photonics

MDPI

Article

Fiber Bragg Grating Bonding Characterization under Long-Period Cyclic Loading

Angela Brindisi [1,*], Cristian Vendittozzi [2], Costanzo Bellini [3], Vittorio Di Cocco [3], Lidia Travascio [4], Luigi Di Palma [5], Marika Belardo [5] and Antonio Concilio [1]

1 Department of Adaptive Structures, CIRA (The Italian Aerospace Research Centre), 81043 Capua, Italy; a.concilio@cira.it
2 Campus FGA-UnB, Universidade de Brasília, Brasília 72444-240, DF, Brazil; vendittozzi@unb.br
3 Department of Civil and Mechanical Engineering, University of Cassino and Southern Lazio, 03043 Cassino, Italy; c.bellini@unicas.it (C.B.); v.dicocco@unicas.it (V.D.C.)
4 Department of Reliability and Safety of Systems and Infrastructure, CIRA (The Italian Aerospace Research Centre), 81043 Capua, Italy; l.travascio@cira.it
5 Department of Airframe Design and Dynamics, CIRA (The Italian Aerospace Research Centre), 81043 Capua, Italy; dplu1973@gmail.com (L.D.P.); m.belardo@cira.it (M.B.)
* Correspondence: a.brindisi@cira.it

Abstract: The Smart Landing Gear system to be developed in the framework of the ANGELA project provides the strain measurements on landing gear structure at landings, and this system should be maintained efficiently under operational conditions. It is intended to assess the relevance of Fiber Bragg Gratings for in-flight testing. To assess the capabilities of the FBG bonding and to analyze the strain transmission conditions from the host structure to the FBG through the bonding layer during the operational phases of landing gears, a long-period cyclic loading test campaign on the bonding layer itself was performed. The primary objective of this fatigue-like test was to prove the ability of FBG sensors to withstand the operational life-cycle of landing gear while providing the same strain transfer function throughout the entire cycle; the secondary objective was to select the most suitable fiber-coating and bonding agents for this application. This document describes the execution and results of the fatigue-like test, intended as a preparatory test campaign to support the preliminary design activities of the Smart Landing System.

Keywords: landing gear; fiber optic sensors; Fiber Bragg Gratings; smart devices; structural health monitoring; fatigue-like test

Citation: Brindisi, A.; Vendittozzi, C.; Bellini, C.; Di Cocco, V.; Travascio, L.; Di Palma, L.; Belardo, M.; Concilio, A. Fiber Bragg Grating Bonding Characterization under Long-Period Cyclic Loading. *Photonics* **2023**, *10*, 906. https://doi.org/10.3390/photonics10080906

Received: 17 July 2023
Revised: 31 July 2023
Accepted: 3 August 2023
Published: 4 August 2023

1. Introduction

For structure health monitoring applications, Fiber Bragg Gratings are among the most promising sensors being used due to their small size, light weight, immunity to electromagnetic interference, multiplexing capabilities, and good resistance to harsh chemicals [1]. While generally, FBGs, when properly customized, have been used to measure humidity, vibrations, pH variation, and even shape, they are mostly used as static sensors to measure temperature and strain [2–4]. By improving acquisition systems and increasing acquisition rates, FBGs are increasingly being used for dynamic applications where gratings are embedded in structures and can monitor engineering devices in real-time without forcing them to stop their operations. FBGs can be embedded in materials in the case of composite laminates or simply bonded to the surface. The latter is still the most widespread solution considering the still-existing difficulties related to the embedding of optical fibers inside metals [5–7]. Even their installation on the outer surface of structures involves some difficulties, particularly for mechanical and thermal strain measurements. When the sensor is bonded to the surface, the strains between the grating and the host structure are expected to be the same without considering that the strain, before being communicated to Bragg

grating, must pass through different media (as in the case of any optical fiber coatings) with different mechanical properties. More specifically, as in the case of traditional strain gauges, an adhesive material is used to install a sensor, resulting in indirect contact between the sensor itself and the monitored structure and leading to variability in the performance of FBGs, especially in harsh environments and under dynamic conditions. To provide good repeatability of the measurements performed by means of FBGs, several researchers are proposing analytical solutions to establish the relationship between the actual deformation of the host structure and that perceived by the surface-bonded grating, attempting to identify the causes of any differences. Experimental measurements based on the Mach–Zehnder interferometric technique were performed to validate the theoretical prediction and reveal the differential strains between the grating and the host structure [8,9]. These parametric studies showed that the percentage of the strain from the host structure actually transferred to the grating depends on the bonding length and the type of adhesive used. The general trend of the strain transfer shows that the longer the bond length and the stiffer the adhesive, the greater the strain transferred to the optical file. The best results were obtained using an epoxy adhesive. Other authors have attempted to identify the critical parameters that affect measurement accuracy, particularly when monitoring mechanical strain, by studying how these parameters affect FBGs sensitivity and accuracy, focusing on the dependence of strain transfer—from the host material to the grating bonded to its surface—on the ratio between the radius of the curvature of the surface and the length of the grating, the equivalent Young's modulus of the sensor, Young's modulus of the host material [10] and the Young modulus of the adhesive, or due to the shear deformation absorbed from the protective coating and adhesive layers [11]. According to the analysis of other authors, the parameters that most interfere with strain transfer are the length and thickness of the adhesive layer over and underneath the fiber [12] and the accuracy in their alignment of the grating, thus parameters related to the accuracy of the installation rather than to material properties [13,14].

The properties of bonding, the proper choice of an adhesive, and the accuracy of installation are characteristics that assume greater importance for dynamic monitoring. In fact, while the acquisition system is able to provide a frequency of acquisition such that it can record the dynamic phenomenon being monitored, allowing its reconstruction with a fine resolution, on the other hand, it is the bonding that must ensure not only a good transfer of deformation from the host structure to the grating but also to maintain the same capacity for the entire duration of the phenomenon being measured.

In a previous paper, the authors analyzed the characteristics of the dynamic response to the impact of model aircraft landing gear with the ground and derived important information to identify hard-impact conditions. For the short-term dynamic test, a set of FBG sensors was installed on the two legs of a scaled landing gear that was subjected to a series of drop tests from various heights using a drop tower [15]. FBGs have demonstrated good sensitivity and repeatability, showing the ability to monitor the phenomenon from the flight phase to impact and to the bounces following it. In this study, it was tested whether FBGs installed on landing gears could monitor the landing phase and detect the type of ground contact to identify the possibility of hard impact. To ensure the operation on real landing gear, the sensor must prove it can survive the design life cycle for the system under analysis by continuing to monitor the system, ensuring the same performance throughout the life cycle.

To simulate the landing gear during the expected landing cycle, it was planned that the FBG would be installed for grating on an aircraft aluminum alloy plate and subjected to a fatigue-like test.

Metal alloys are used to manufacture many types of parts, such as rods, casings, beams, and pillars, for employment in various kinds of structures. Most of these structures are subjected to histories of severe cyclic loading, which raises the risk of fatigue-damaging mechanisms' activation and the subsequent failure of the components [16]. In the past, several investigators have studied the fatigue behavior of metal alloys. Slamecka and

Pokluda [17] implemented an empirical method to estimate the fatigue behavior of parts subjected to rotational loads based on a quadratic equivalent-stress formula and validated this by a comparison with data from different materials. Shen et al. [18] carried out low-cycle fatigue tests on specimens extracted along different directions from a wheel to study the effect of the extrusion direction. An effect of this direction on both fatigue and static behavior was found due to the different microstructures. The impact of the microstructure was investigated by Iacoviello et al. [19] too, who analyzed the effect of the graphite nodules on the fatigue crack propagation in ductile cast iron. The same authors examined the impact of overload on crack propagation under fatigue loading, taking into consideration the material microstructure too [20]. Benachour et al. [21] studied the effect of notches on crack initiation to predict the residual lifetime in aeronautical structures through numerical and experimental investigations. A comprehensive experimental study was carried out by Zupanic et al. [22] to determine the fatigue and mechanical characteristics of a commercial aluminum alloy, finding a high fatigue strength for both low-cycle and high-cycle tests. Yankin et al. [23] proposed a modified model to predict the effect of multiaxial fatigue loads on the 2024 aluminum alloy and validated it by a comparison against experimental data. Different studies have been carried out for monitoring and predicting the failure of parts due to fatigue loading. Acoustic emission testing was adopted by D'Angela et al. [24,25] to determine the damaging micromechanics in ductile cast iron, correlating its mechanical behavior to the evolution of acoustic emissions and recommending a failure criterium. Cui et al. [26] proposed a thin film strain gauge to be applied in high-temperature environments that were built using platinum–rhodium films. They carried out several experimental tests to find the best solution for the thermal insulation of the sensor. Kordell et al. [27] ideated a surface-mounted fiber optic conjugate stress sensor to evaluate the modulus of specimens under plastic deformation and tested this on different types of metals.

The results discussed in the present paper have been developed for the Smart Landing Gear (SLG) system, which is one of the innovations "beyond the state of the art" to be developed in the framework of the ANGELA project, funded by the CS2 platform, Fast Rotorcraft IADP. This activity foresees the design and development of a Smart Landing Gear system for Hard Landing detection based on Fiber Optic Sensor technology to be integrated into the Landing Gear structure [15,28]. The Smart Landing Gear system provides strain measurements on the landing gear structure at landings, and this system should be maintained efficiently under operational conditions. It is intended to assess the relevance of Fiber Bragg Gratings (FBG) for in-flight testing.

In this paper, the fatigue-like test was intended solely to verify whether the sensor installed on its surface could withstand the cyclic test and not analyze the behavior of metal plates. Herein, fatigue-like is meant as a test that uses the principles of fatigue testing to study the behavior of bonding using long-period cyclic loading to verify that no decay of the bonding properties has occurred. Thus, the object of the analysis was to evaluate whether the bonding could ensure the same transfer function from the first to the last cycle of the test, continuing to monitor the deformation of the metal plate all the time with the same efficiency. Two adhesive agents, including cyanoacrylate and epoxy, and two fiber coatings, polyimide, and acrylate, were investigated in the same test. To assess the capabilities of the sensor bonding to verify the strain transmission conditions from the structure to the FBG sensor through the bonding layer during the operational phases of landing gear, a fatigue-like test campaign on the bonding layer itself was performed, and results are hereafter discussed.

2. Materials and Methods

The fatigue-like tests discussed here have two objectives. The first objective was to prove the ability of FBG sensors to withstand the operational life cycle of landing gear while maintaining its sensitivity, and the second one was to select the most suitable fiber-coating and bonding agents for this application.

Since there is not a specific accepted standard for our purpose, a modified version of the test defined by ASTM D3166-99 [29] could be used. ASTM D3166-99 is referred to as a test method for fatigue properties of the adhesive in shear by tension loading in a metal-to-metal junction. For our purposes, the adhesive would not be used for a permanent junction between two metal plates but as a bonding element between the fibers at the metal plate; therefore, a single plate configuration was considered. This configuration, depicted in Figure 1, allows the sensitivity of the installed sensors to be measured by making the specimen undergo cyclic displacements while testing two different types of adhesives in combination with two different types of fiber coating. The single-plate configuration provides verification of the operating life of the installed sensors compared to the operating life of the substrate.

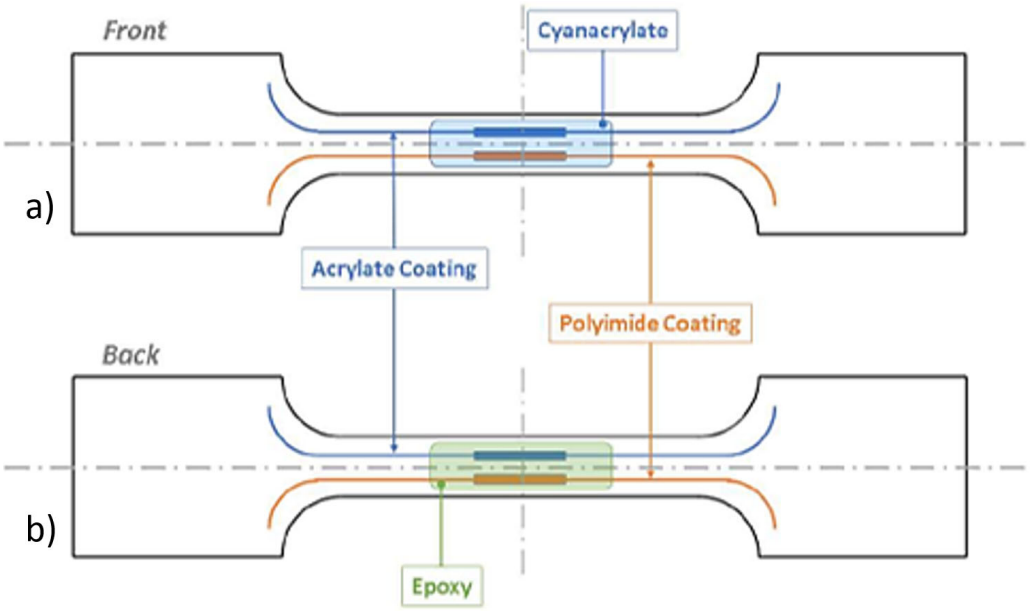

Figure 1. (**a**) Front and (**b**) Back sides of a dog–bone specimen showing the acrylate and polyamide fiber coatings, and the two different bonding agents: epoxy (in green) and cyanoacrylate (in blue).

The specimen material must comply with that used on the landing gear to which FBGs are installed. This is because the chemical and physical characteristics of the material surfaces affect the behavior of the adhesive layer. The used specimens are made of an aircraft-grade aluminum alloy plate (Al7075-T7351).

The two different bonding agents that are compared are a cyanoacrylate cold-curing superglue structural adhesive (HBM Z70) and a bi-component cold-curing epoxy (Bostik High-Speed Steel). Both can work in the temperature range of −55 °C to 120 °C, as prescribed by the project requirements.

In this configuration, on the front side of the specimen, two fibers, one with the acrylate coating and the other with the polyimide coating, are bonded with cyanoacrylate, while on the back side, two more fibers with the same coatings as on the front side are instead bonded with epoxy, as shown in Figure 1.

The recommended geometry of the specimen is a classical dog bone type, wider at the grips and narrower in the central part where the sensors are bonded. The plate thickness must be contained to allow the application of controlled and effective loads; excessive loads could adversely affect the tests. In Figure 2, the specimen's shape and dimensions are illustrated.

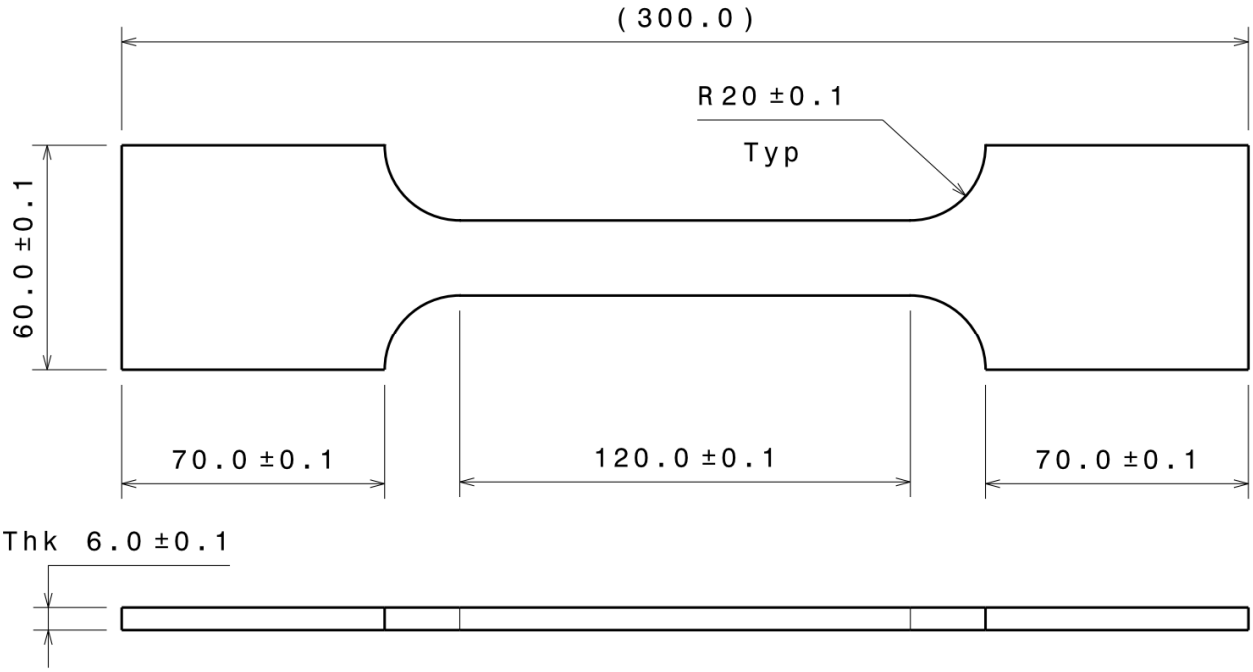

Figure 2. Dog-bone specimen: shape and dimensions. All dimensions are in millimeters (mm).

The set of dog-bone specimens was composed of 5 specimens, named A, B, C, D, and E, respectively. Four FBGs, 15 mm in length, were bonded on each specimen, two on each face with the same type of adhesive. The gratings were apodized FBGs (reflectivity $\geq$ 75%) directly written, with the excimer laser, on 9/125 single-mode optical fiber, which was locally stripped and then re-coated. The fibers were bonded on the specimen's faces alternating the central wavelengths (CWL) of 1530 nm and 1550 nm with the fiber coatings, polyimide, and acrylate. Table 1 illustrates the configuration for each specimen side, including the CWLs, the coatings, and the glues.

Table 1. Dog–bone specimens' bonded FBGs configuration.

Sensor Reference	Specimen	Side	CWL (nm)	Coating	Glue
A1	A	Front	1530	Acrylate	Epoxy
A2	A	Front	1550	Polyimide	Epoxy
A3	A	Back	1530	Acrylate	Cyanoacrylate
A4	A	Back	1550	Polyimide	Cyanoacrylate
B1	B	Front	1530	Acrylate	Epoxy
B2	B	Front	1550	Polyimide	Epoxy
B3	B	Back	1530	Acrylate	Cyanoacrylate
B4	B	Back	1550	Polyimide	Cyanoacrylate
C1	C	Front	1530	Acrylate	Epoxy
C2	C	Front	1550	Polyimide	Epoxy
C3	C	Back	1530	Acrylate	Cyanoacrylate
C4	C	Back	1550	Polyimide	Cyanoacrylate
D1	D	Front	1530	Acrylate	Epoxy
D2	D	Front	1550	Polyimide	Epoxy
D3	D	Back	1530	Acrylate	Cyanoacrylate
D4	D	Back	1550	Polyimide	Cyanoacrylate
E1	E	Front	1530	Acrylate	Epoxy
E2	E	Front	1550	Polyimide	Epoxy
E3	E	Back	1530	Acrylate	Cyanoacrylate
E4	E	Back	1550	Polyimide	Cyanoacrylate

The installation of the sensors on the specimens was carried out with care under controlled temperature and humidity. Each bonding was then covered with a thin layer of transparent silicone to provide protection from minor impacts and moisture from the surrounding environment. The polymers used as coatings, primarily polyimide, were hygroscopic. This ability to absorb moisture from the environment could greatly affect the performance of the gratings. Figure 3 illustrates the transparent layer of silicone on the epoxy (black) adhesive on a specimen.

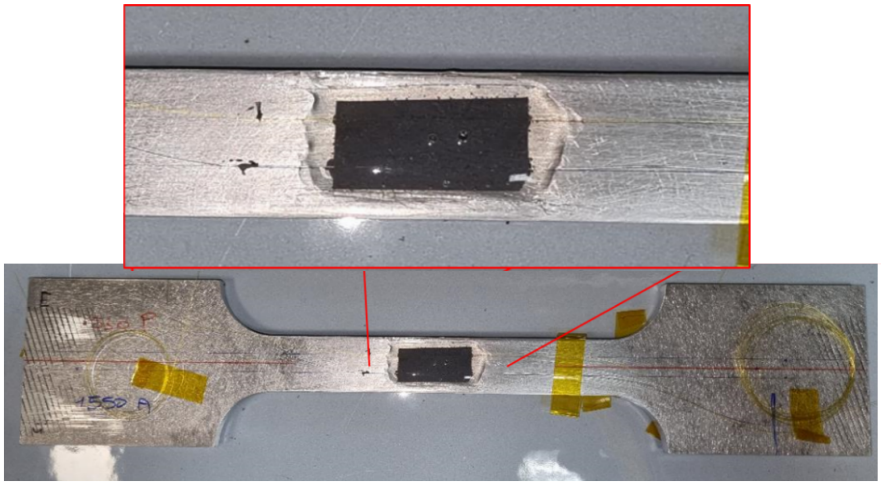

Figure 3. A transparent silicone layer was applied to the bonding agent to protect the FBG from moisture and any small incidental impacts.

The combination of the cyanoacrylate glue with the acrylate fiber coating caused, during the bonding process, the uneven dissolving of the coating: the adhesive acted like a solvent. Figure 4 shows the effect of the adhesive agent on the coatings. As it is shown, the fiber was partially or completely stripped. This irregularity showed up as an uneven and non-uniform reading from these gratings. The cyanoacrylate did not affect the polyimide fiber coating.

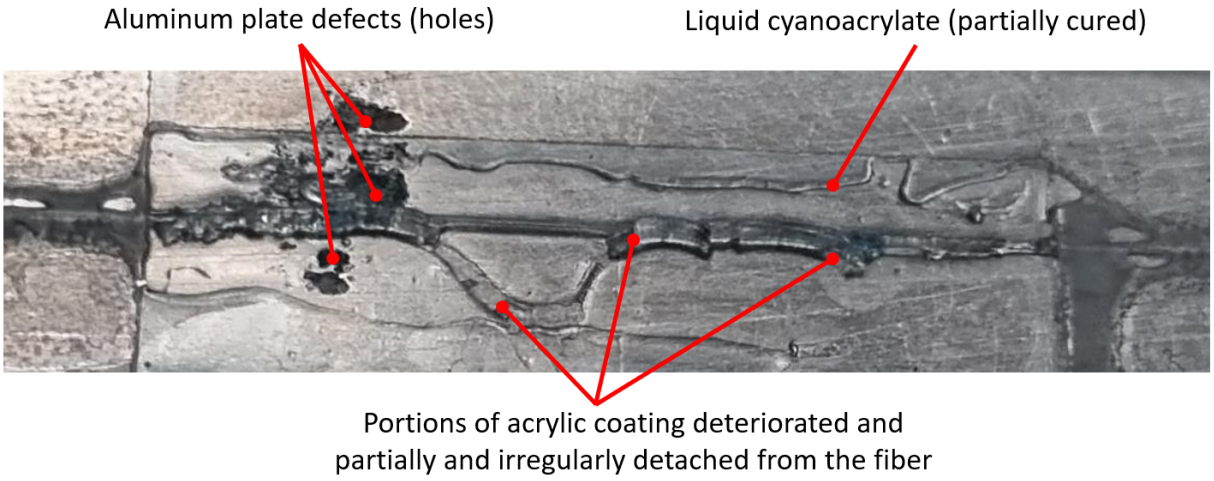

Figure 4. Effect of the cyanoacrylate adhesive on the acrylate fiber coatings.

Test Equipment

The FBG signals were acquired with Micron Optics sm130 Optical Sensing Interrogator using an acquisition rate of 100 Hz. The interrogator was equipped with 4 channels that were capable of acquiring the same rate at the same time. Hence, the 4 FBGs on each specimen were acquired simultaneously.

A fatigue testing machine capable of applying required cyclic loads was used. The electromechanical tensile testing machine used was a Galdabini 1890 (Figure 5), which was equipped with a 100 kN load cell. Each cycle was counted starting from zero (S_{min}), which corresponded to the specimen in the initial position, to the maximum load required (S_{MAX}), and its subsequent release until its return to the starting condition. This provided the load range (S_{Range}) as the maximum applied load.

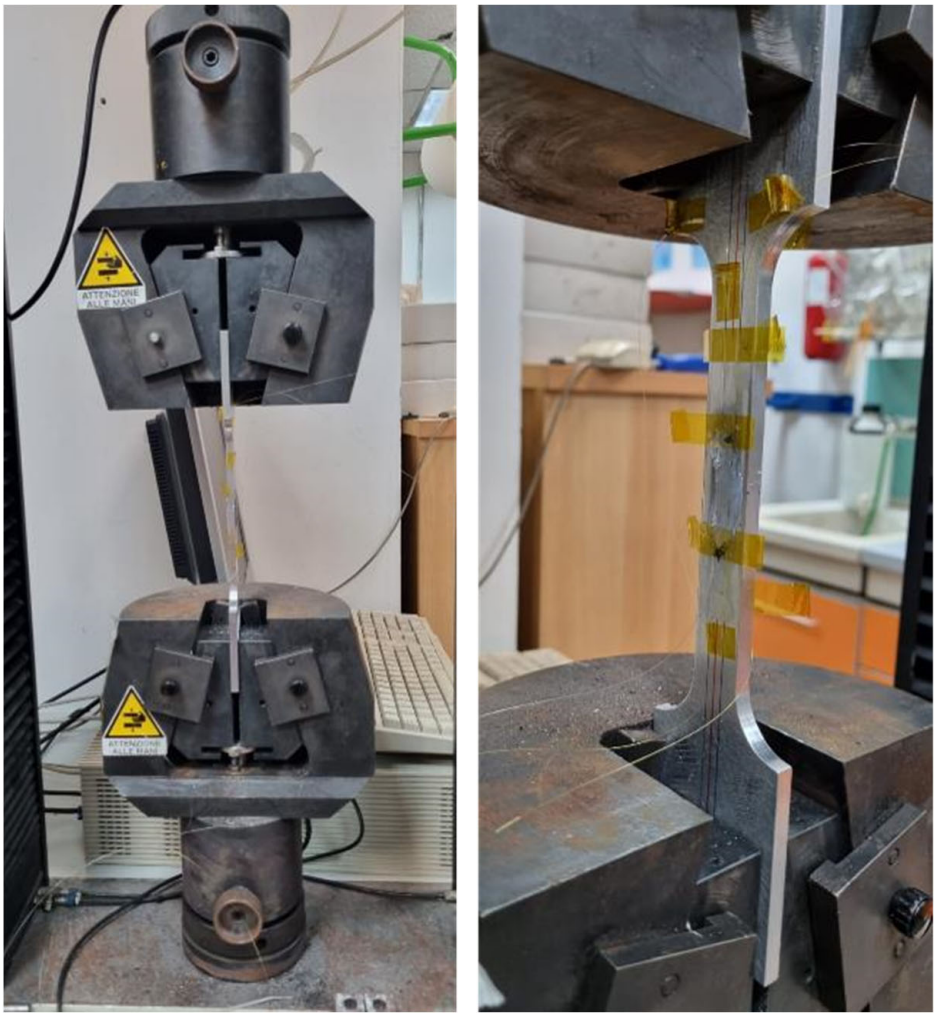

Figure 5. Tensile testing machine: Galdabini 1890 equipped with a 100 kN load cell. A specimen integrated with the 4 fibers is clamped.

The specimens were subjected to deformation cycles that kept them in the elastic range, thus setting the maximum load within 75–80% of the Yield Strength (σ_Y).

According to the project requirements, the transmission of the strain from the structure to the FBG sensors should be maintained efficiently for at least 500 h of safe flight (SFH, Safe Flight Hours); during each hour, 10 landings were expected to occur on average. The number of cycles (n) per SFH package was therefore identified as five thousand (n= 5000).

The machine applied cyclic stress to the specimen, consisting of 5000 repetitions, starting from zero up to a maximum load value of 35.4 kN, which corresponded to 77% of the σ_Y of the used aluminum alloy. This load was chosen to be sufficiently representative for the required cyclic test while respecting certain safety issues. Therefore, it represented a significant fraction of the yield stress, which could avoid sample breakage during the tests and provide an adequate level of stress.

In Table 2 the values of the parameters characterizing the test are listed.

Table 2. Summary of test parameters.

Number of Cycles (*n*)	5000
Material	Al7075-T7351
σ_Y	393 MPa
E	71.7 GPa
σ_{MAX} = 77% σ_Y	295 MPa
S_{MAX} (Maximum Applied Load, @ σ_{MAX})	35.4 kN
Expected Maximum Strain (σ_{MAX}/E)	4.1×10^3 με
Test Speed	20 mm/min
Frequency	0.26 Hz
Test Duration	19,230.8 s
Average Cycle Duration	3.85 s

3. Test Execution and Results

The present test was evaluated in terms of the strains recorded by the FBGs in response to the applied load, so consequently, we refer to a range of the strains (ε_{Range}) calculated as the difference between the maximum (ε_{Max}) and minimum (ε_{min}) strains measured during the cycling test, as shown in Figure 6.

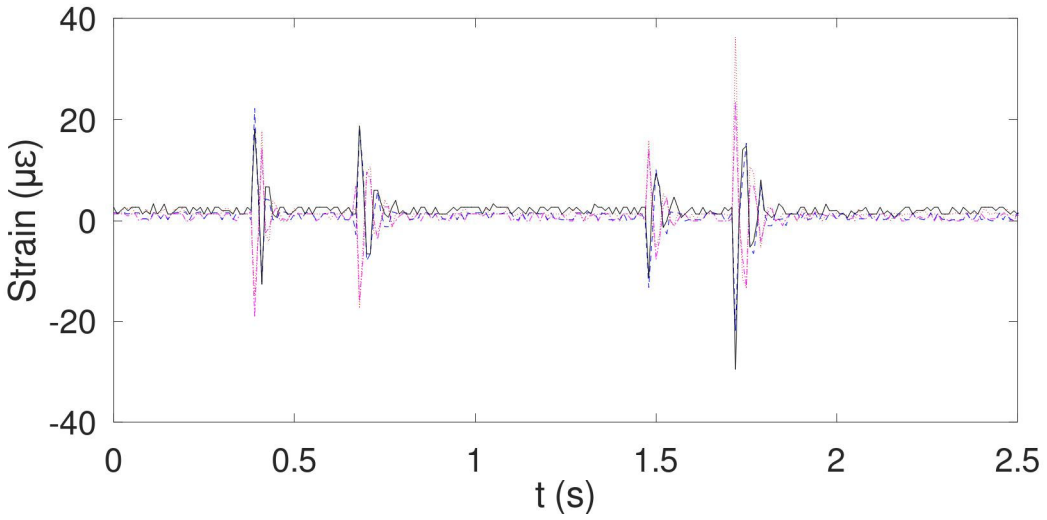

Figure 6. Series of four hits (impulsive load) that were applied to specimen A to verify the simultaneity of the response of the 4 gratings. As the gratings located on the front face were stretched, the gratings located on the back face were compressed and vice versa. The grating A1 is illustrated by the solid black line, A2 by the dashed line in blue, A3 by the dotted line in red, and A4 by the dash-dotted line in magenta (reference Table 2).

Calibration was required to select the test settings, such as the test speed (i.e., the lifting speed of the traction machine up to the required maximum load), test the frequency (i.e., the number of cycles per second), and the FBGs' signal acquisition rate.

In order to verify the simultaneity of the response of the four gratings, a series of four hits (impulsive load) were applied to the specimens. As the gratings located on the front face were stretched, the gratings located on the back face were compressed, and vice versa (Figure 6).

The first step of the test execution was the calibration of the tensile machine, which was performed by using specimen A and running several sessions of about 3000 cycles each to identify the best test settings (Figure 7). Specimen A resulted at the end of the calibration in appearing overstressed and was then discarded for further tests.

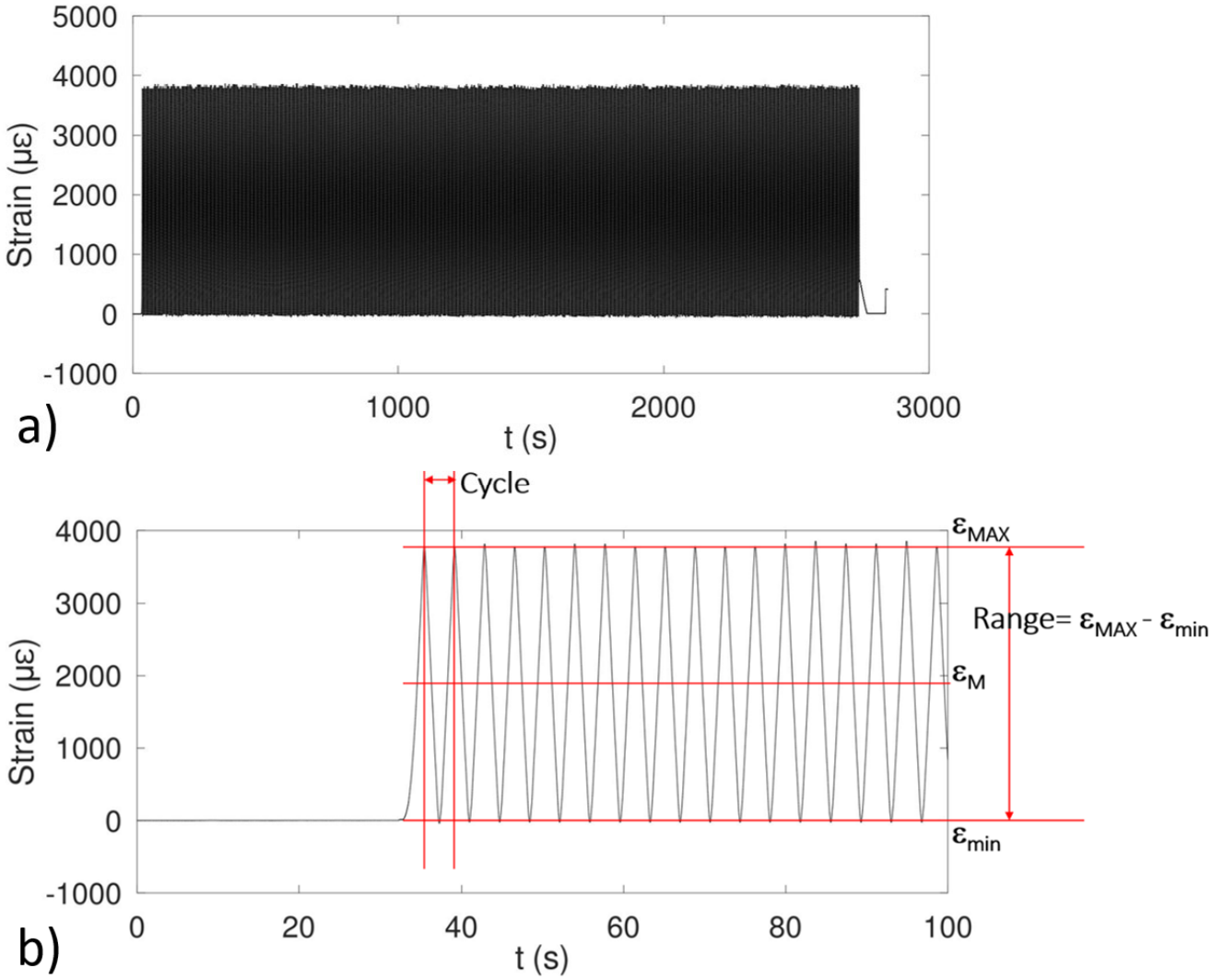

Figure 7. (**a**) Cyclic strain measured at specimen A for 2800 s. (**b**) Zoom of the first 100 s of the previous graph.

The metal specimens had some surface defects that could not be removed by polishing them and could cause the local shrinking of the thickness of the samples; this imposed a rather low test speed (20 mm/min), resulting in a frequency of 0.26 Hz and a total duration for each test of about 5 h and 30′.

A total of four tests were performed: the tensile machine applied a cycling signal to each of the four specimens B, C, D, and E, and the resulting strains were recorded by the FBGs in response to the applied loads.

The loadcell graphs of the four specimens B, C, D, and E, show the typical sinusoidal trend of the cyclic test from about 0 kN to 35.4 kN (Figure 8). Sample C graph shows a shorter duration because specimen C crashed after 18,291.180 s. This failure was due to the presence of an inclusion that weakened the specimen's resistant section.

The strains recorded by the FBG sensors, in response to the applied loads to specimens B, C, D, and E, are shown in Figures 9–12, respectively. The FBGs' signals, following the scheme shown in Table 1, indicated the combination of the sensor coating and bonding agent: (1) Acrylate–Epoxy, (2) Polyimide–Epoxy, (3) Acrylate–Cyanoacrylate, and (4) Polyimide–Cyanoacrylate. The red dashed line indicates the expected maximum value of the strain (Table 2).

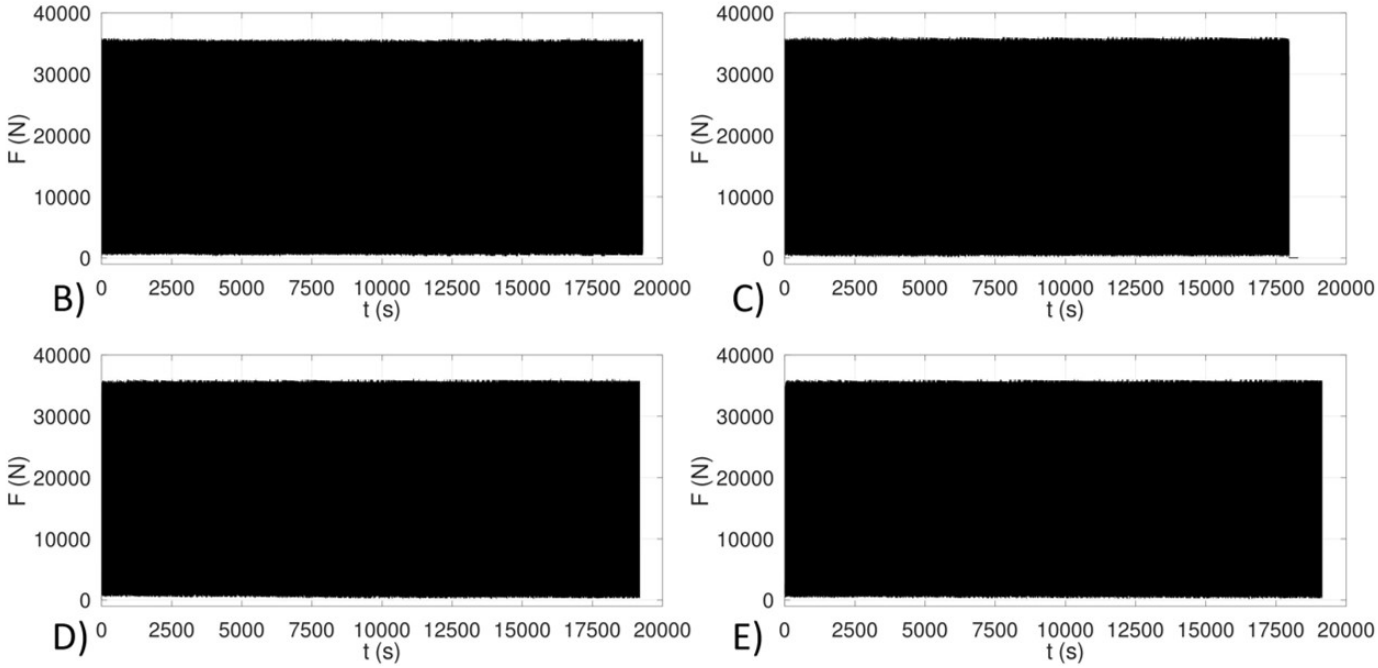

Figure 8. Measure by the load cell of the applied loads for the 4 specimens, B, C, D, and E (cyclic test 0 to 35.4 kN).

The FBG signals acquired during the fatigue-like tests for all the specimens provided, in general, consistent responses with the respective applied loads. The acquired signal followed very well in time with the cyclic behavior of the applied loads. Some discrepancies instead were present in the amplitudes of the signals between the signals and the expected maximum values and depended mainly on the combination of the sensor coating and bonding agent of the sensors. In particular, the acrylate–epoxy combination exhibited for all the specimens, namely for the sensors B1, C,1, D1, and E1, provided the worst transfer functions.

With regard to specimen B, Figure 9 shows a small irregularity during the first 5000 s of the test for all the sensors, probably due to the slight settling of the specimen in the clamps of the tensile-test machine. After settling, the signals showed no further variation until the end of the test. Considering specimen C, Figure 10 shows the signal response of FBGs in a stable range throughout the test, which suddenly stopped due to specimen rupture, as anticipated in the previous section, after completing 95.1% of the expected duration. Figure 11 shows the grating plots of specimen D. The four signals showed a constant range throughout the test. Only sensor D3 exhibited a signal oscillation between 3500 and 7000 s. Initially, the signal presented an ε_{max}, on average, of about 4500 $\mu\varepsilon$, which later decreased to about 4200 $\mu\varepsilon$. Despite this variation, the ε_{range} remained practically constant because the ε_{min} was in the first phase, about 50 $\mu\varepsilon$, while in the second phase, it dropped to about -150 $\mu\varepsilon$. This behavior could be caused by the slippage of the optical fiber within the adhesive layer, which was induced by the imperfect adhesion between the layers that transferred the strain to the grating, namely, between the adhesive agent and the coating and between the coating itself and the fiber. Specimen E, whose results are shown in Figure 12, showed no significant fluctuations during the test, and the four gratings recorded an almost constant range.

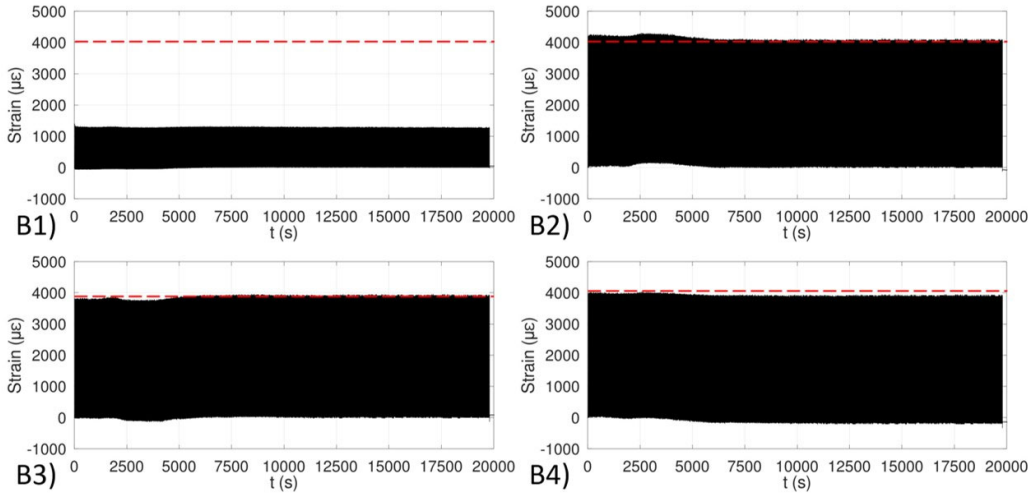

Figure 9. Measured strain by the 4 FBGs on specimen B: (1) Acrylate-Epoxy, (2) Polyimide–Epoxy, (3) Acrylate–Cyanoacrylate, and (4) Polyimide–Cyanoacrylate.

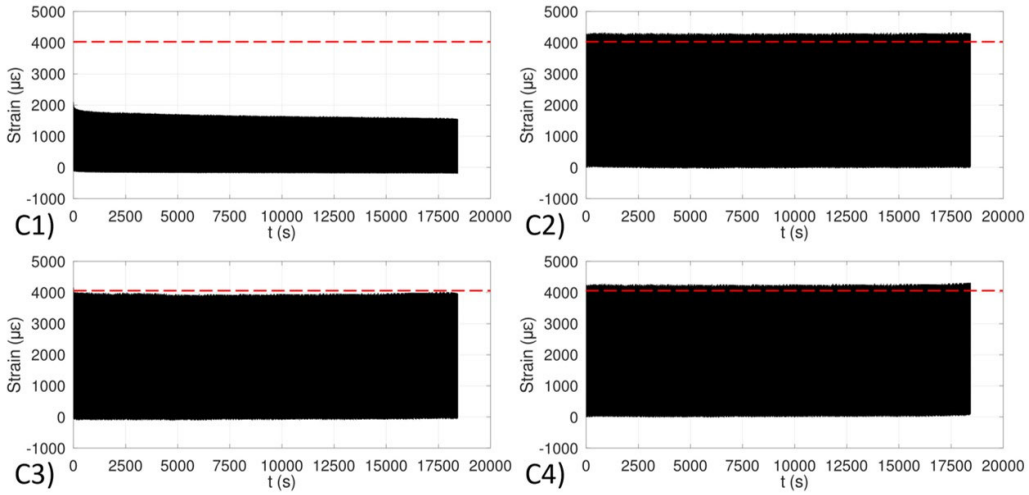

Figure 10. Measured strain by the 4 FBGs on specimen C: (1) Acrylate–Epoxy, (2) Polyimide–Epoxy, (3) Acrylate–Cyanoacrylate, and (4) Polyimide–Cyanoacrylate.

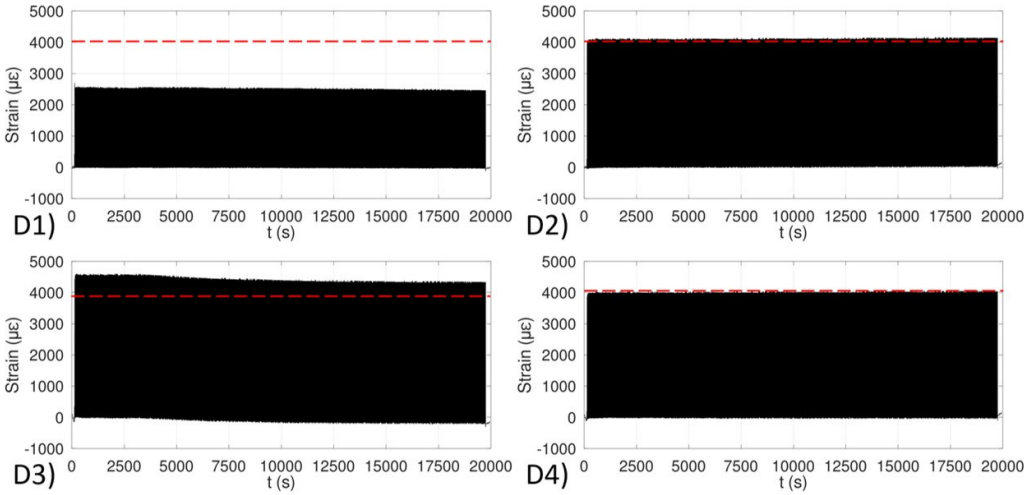

Figure 11. Measured strain by the 4 FBGs on specimen D: (1) Acrylate–Epoxy, (2) Polyimide–Epoxy, (3) Acrylate–Cyanoacrylate, and (4) Polyimide–Cyanoacrylate.

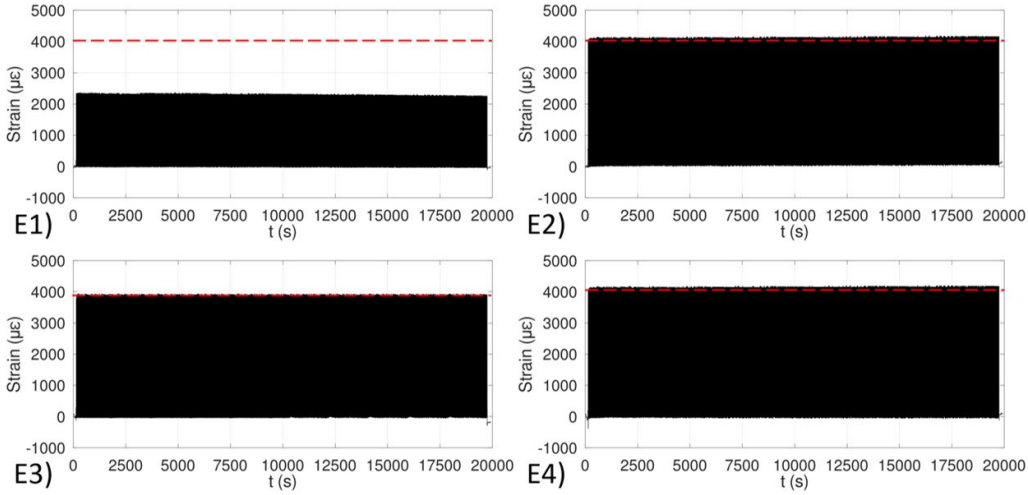

Figure 12. Measured strain by the 4 FBGs on specimen E: (1) Acrylate–Epoxy, (2) Polyimide–Epoxy, (3) Acrylate–Cyanoacrylate, and (4) Polyimide–Cyanoacrylate.

Table 3 summarizes the ε_{Range} values calculated as the difference between the ε_{max} and ε_{min} deduced from the graphs shown in Figures 9–12. These data allow the construction of the graph in Figure 13, which shows a comparison of the ε_{Range} recorded by each FBG bonded to the four specimens and, more importantly, of the four combinations of the sensor coating and bonding agent: (1) Acrylate–Epoxy (blue histogram), (2) Polyimide–Epoxy (yellow histogram), (3) Acrylate–Cyanoacrylate (gray histogram), and (4) Polyimide–Cyanoacrylate (orange histogram).

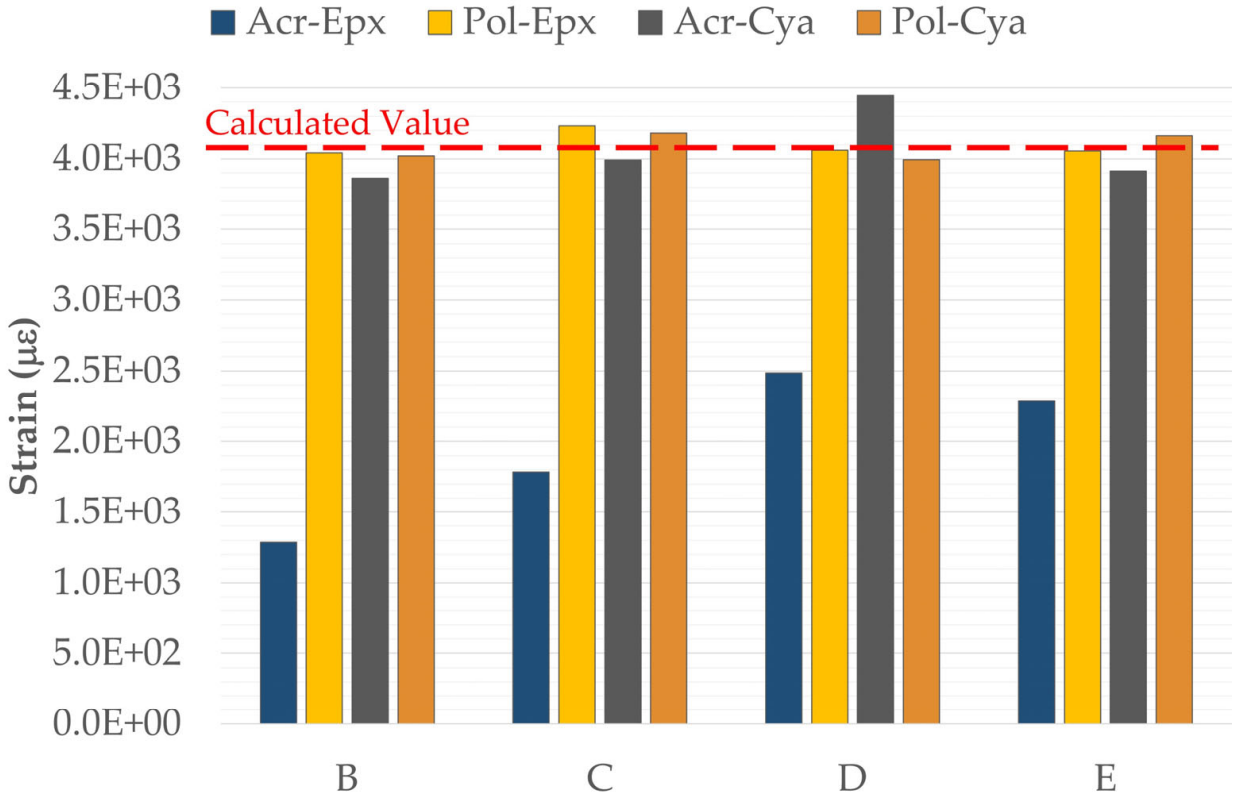

Figure 13. Comparison between ε_{Range} and expected maximum strains for each sensor for the specimens B, C, D, and E.

Table 3. Values of $\varepsilon_{Range} = \varepsilon_{max} - \varepsilon_{min}$. All values are given in microstrain (με).

	ε_{Max}	ε_{min}	ε_{Range}		ε_{Max}	ε_{min}	ε_{Range}
B1	1288.394	3.337	1285.057	**D1**	2470.047	−16.481	2486.527
B2	4076.907	33.051	4043.856	**D2**	4091.460	29.788	4061.672
B3	3889.732	25.379	3864.353	**D3**	4341.352	−104.583	4445.935
B4	3878.169	−145.070	4023.239	**D4**	3980.511	−15.743	3996.254
C1	1612.708	−172.835	1785.543	**E1**	2267.650	−17.309	2284.959
C2	4246.952	14.081	4232.872	**E2**	4107.759	51.922	4055.837
C3	3939.832	−83.608	4023.439	**E3**	3882.692	−31.301	3913.993
C4	4212.620	31.122	4181.498	**E4**	4131.502	−29.690	4161.192

Figure 13 aims to compare the performance of the proposed adhesive agent-coating combinations to verify the magnitude of the transfer function, the applied load vs. the measured strain, and the repeatability of the integration process. Finally, the reliability of the bonding, i.e., the level of slippage of the grating with respect to the structure, was preliminarily evaluated.

4. Discussion

The behavior of the polyimide coating, regardless of the type of bonding agent used, showed a performance that was always consistent with the expected strain of the specimen. In particular, the polyimide–epoxy combination (shown in yellow in Figure 13) exhibited a deviation from the expected value of 1.71%, 2.88%, 1.28%, and 1.42% on specimens B, C, D, and E, respectively. For the polyimide–cyanoacrylate combination, the deviations from the expected value were 2.21% for specimen B, 1.63% for specimen C, 2.87% for specimen D and 1.14% for specimen E. Deviations are reported in absolute value. Acrylate-coated gratings, on the other hand, showed a performance that was not always consistent with the actual deformation of the specimen.

The Acrylate–Epoxy combination exhibited the worst transfer function, with deviations from the expected value of 68.77%, 56.60%, 39.56%, and 44.46% for specimens B, C, D, and E, respectively. The grating appeared to be partially isolated and did not consistently sense the deformations of the specimen to which they were bonded. It should be remembered that what was improperly referred to as a "polymer jacket" was actually just a tight jacket that was directly in contact with the optical fiber. The transfer function of the FBG is highly dependent on the bonding ability (i.e., the interfacial strength between acrylate and fused silica substrate) of this jacket to the fiber. It is assumed that the possible better adhesion of the epoxy to the acrylic coating, compared to that between the same acrylic jacket and the fused silica fiber, might have caused a relative slippage in the fiber within the jacket, altering the sensitivity of the grating.

For the Acrylate–Cyanoacrylate combination, strains were also recorded with a more variable deviation from the expected value, i.e., 6.08% for specimen B, 2.95% for C, 8.06% for D, and 4.87% for E. It was assumed that the cause of this non-uniformity could be ascribed to the problem encountered during bonding. Cyanoacrylate acted as a solvent for the acrylic coating, which deteriorated rapidly as the adhesive cured, Figure 5. This degradation was not uniform; in fact, along 15 mm of the grating, in some locations, the cladding seemed undamaged and adherent to the fiber; in other locations, the fiber was completely stripped. In some locations, the damaged coating overlapped with the fiber, and in others, it was the fiber that overlapped with the removed portion of the coating. These different configurations, all concentrated in a short stretch of only 15 mm, might have induced the uneven acquisition of the grating strain. The fully stripped parts were probably the ones that best transferred the strain to the grating.

During the execution of each test, which lasted about five and a half hours, while simulating 5000 cycles, the protective silicone layer covering the sensors seemed to work effectively.

5. Conclusions

In the framework of the development of the Smart Landing Gear system and in order to assess the relevance of Fiber Bragg Gratings for in-flight testing, the tests described in the present paper have been conducted with the objective of proving the ability of FBG sensors to withstand the operational life cycle of landing gear while maintaining its sensitivity and to select the most suitable fiber-coatings and bonding agents for this application. In fact, an essential aspect of the FBG integration is the bonding of the sensor to the structure with a bonding agent, which, in turn, has to transfer all the deformation of the hosting structure to the sensing element and has to withstand the operational life cycle of the landing gear and also provide the same transfer function throughout the entire cycle. Regardless of the used coatings and adhesives, the four gratings were able to record the strains from the beginning to the end of each test and for each specimen. The sensor signals followed in time the cyclic applied load very well. In the case of specimen C, the sensor survived the same specimen crashing due to an internal defect in the material.

Some discrepancies were present in the amplitude of the signal, and the transfer function gave a result far from the expected one depending on the fiber-coating and bonding agent combinations. In particular, the acrylic combination (cyanoacrylate on acrylate coating), due to the problem encountered with the coating, unevenly deteriorated and provided the worst transfer function of deformation and was therefore excluded from the next steps of SLG development. The combination of acrylate coating and epoxy glue also did not give an acceptable result due to variability in the results. In general, it seems that the acrylate fiber coating does not allow the adequate transfer of the actual strain from the deformed specimen to the FBG. It would appear that, during cyclic testing, the adhesive agent drags the coating, and this does not allow a complete strain transfer to the grating. The polyimide coating showed consistent results on all tested specimens, both in combination with epoxy and cyanoacrylate and performing better than acrylate coatings. In fact, regardless of the used bonding agent, the strain measured by the two polyimide recoated gratings—for each specimen—provided almost overlapping results.

The bonding stability was tested over the required number of cycles. The bonding performance was stable to a large extent; therefore, the extremely limited variability does not allow the extrapolation of a general law regarding the temporal behavior of the bondings over a long period exceeding the required number of cycles.

The test was conducted in a temperature-controlled laboratory, maintaining a constant temperature throughout the duration of testing. In the future, a climatic chamber test should also be performed, simulating an operating environment where temperature and moisture can vary.

Author Contributions: Conceptualization, A.B.; methodology, C.V.; software, C.V.; validation, A.B. and C.V.; formal analysis, A.C.; investigation, C.B. and V.D.C.; resources, L.D.P. and L.T.; data curation, C.V. and A.B.; writing—original draft preparation, A.B. and C.V.; writing—review and editing, A.C.; visualization, A.B. and C.V.; supervision, L.T.; project administration, L.D.P. and M.B.; funding acquisition, A.C. and L.D.P. All authors have read and agreed to the published version of the manuscript.

Funding: The research leading to these results has gratefully received funding from Clean Sky 2 Joint Undertaking under the European Union's Horizon 2020 research and innovation program under the Grant Agreement for members GAM-2020-FRC—H2020-IBA-CS2-GAMS-2019/H2020-IBA-CS2-GAMS-2019 Amendment Reference No AMD-945542-22.

Institutional Review Board Statement: Not applicable.

Informed Consent Statement: Not applicable.

Data Availability Statement: The data are not publicly available due to confidentiality reasons.

Conflicts of Interest: The authors declare no conflict of interest.

References

1. Udd, E. Fiber optic smart structures. *Proc. IEEE* **1996**, *84*, 884–894. [CrossRef]
2. Friebele, E.J. Fiber Bragg Grating Strain Sensors: Present and Future Applications in Smart Structures. *Opt. Photonics News* **1998**, *9*, 33. [CrossRef]
3. Riza, M.A.; Go, Y.I.; Harun, S.W.; Maier, R.R.J. FBG Sensors for Environmental and Biochemical Applications—A Review. *IEEE Sens. J.* **2020**, *20*, 7614–7627. [CrossRef]
4. Wu, J.; Li, B.; Li, C.; Qiu, Y.; Zhang, Z.; Lyu, W.; Ali, A.; Mohsan, S.A.H.; Ge, W.; Tong, Z.; et al. Fiber Bragg grating-based shape sensing: A review and perspective. In Proceedings of the Global Intelligent Industry Conference, Guangzhou, China, 17–19 November 2020; SPIE: Bellingham, WA, USA, 2021; Volume 11780. [CrossRef]
5. Li, X.C.; Prinz, F.; Seim, J. Thermal behavior of a metal embedded fiber Bragg grating sensor. *Smart Mater. Struct.* **2001**, *10*, 575–579. [CrossRef]
6. Lindner, M.; Stadler, A.; Hamann, G.; Fischer, B.; Jakobi, M.; Heilmeier, F.; Bauer, C.; Volk, W.; Koch, A.W.; Roths, J. Fiber Bragg Sensors Embedded in Cast Aluminum Parts: Axial Strain and Temperature Response. *Sensors* **2021**, *21*, 1680. [CrossRef]
7. Grandal, T.; Zornoza, A.; Fraga, S.; Castro, G.; Sun, T.; Grattan, K.T.V. Laser Cladding-based metallic embedding technique for fiber optic sensors. *J. Light. Technol.* **2018**, *36*, 1018–1025. [CrossRef]
8. Piñeiro, E.; Grandal, T.; Asensio, A.; Rodriguez, F. Coating process of Fiber Bragg Grating sensors for SHM applications in metallic structures. In Proceedings of the SPIE 9157, 23rd International Conference on Optical Fibre Sensors, Santander, Spain, 2 June 2014; SPIE: Bellingham, WA, USA, 2014; Volume 9157. [CrossRef]
9. Her, S.-C.; Huang, C.-Y. The Effects of Adhesive and Bonding Length on the Strain Transfer of Optical Fiber Sensors. *Appl. Sci.* **2016**, *6*, 13. [CrossRef]
10. Floris, I.; Madrigal, J.; Sales, S.; Adam, J.M.; Calderón, P.A. Experimental Study of the Influence of FBG Length on Optical Multicore Shape Sensors Performance. In Proceedings of the Asia Communications and Photonics Conference (ACP), Chengdu, China, 2–5 November 2019; pp. 1–3.
11. Floris, I.; Sangiorgio, V.; Adam, J.M.; Uva, G.; Rapido, M.; Calderón, P.A.; Madrigal, J. Effects of bonding on the performance of optical fiber strain sensors. *Struct. Control Health Monit.* **2021**, *28*, e2782. [CrossRef]
12. Wan, K.T.; Leung, C.K.Y.; Olson, N.G. Investigation of the strain transfer for surface-attached optical fiber strain sensors. *Smart Mater. Struct.* **2008**, *17*, 035037. [CrossRef]
13. Zhou, J.; Zhou, Z.; Zhang, D. Study on Strain Transfer Characteristics of Fiber Bragg Grating Sensors. *J. Intell. Mater. Syst. Struct.* **2010**, *21*, 1117–1122. [CrossRef]
14. Wan, K.T. Quantitative Sensitivity Analysis of Surface Attached Optical Fiber Strain Sensor. *IEEE Sens. J.* **2014**, *14*, 1805–1812. [CrossRef]
15. Brindisi, A.; Vendittozzi, C.; Travascio, L.; Di Palma, L.; Ignarra, M.; Fiorillo, V.; Concilio, A. A Preliminary Assessment of an FBG-Based Hard Landing Monitoring System. *Photonics* **2021**, *8*, 450. [CrossRef]
16. Bellini, C.; Di Cocco, V.; Favaro, G.; Iacoviello, F.; Sorrentino, L. Ductile cast irons: Microstructure influence on the fatigue initiation mechanisms. *Fatigue Fract. Eng. Mater. Struct.* **2019**, *42*, 2172–2182. [CrossRef]
17. Slámečka, K.; Pokluda, J. Simple criterion for predicting fatigue life under combined bending and torsion loading. *Frat. Ed Integrita Strutt.* **2017**, *11*, 123–128. [CrossRef]
18. Shen, Z.; Yang, L.; Deng, J.; Zhu, Y.; Su, Y. Low-cycle fatigue characteristics and fracture behavior of the die-forged 2014 aircraft wheel. *Fatigue Fract. Eng. Mater. Struct.* **2023**, *46*, 295–309. [CrossRef]
19. Iacoviello, F.; Di Cocco, V.; Bellini, C. Fatigue crack propagation and damaging micromechanisms in Ductile Cast Irons. *Int. J. Fatigue* **2019**, *124*, 48–54. [CrossRef]
20. Iacoviello, F.; Di Cocco, V.; Bellini, C. Overload effects on fatigue cracks in a ferritized ductile cast iron. *Int. J. Fatigue* **2019**, *127*, 376–381. [CrossRef]
21. Benachour, N.; Benachour, M.; Benguediab, M. Experimental investigation of fatigue crack initiation from notches in 2024 T351 al-alloy. *Frat. Ed Integrita Strutt.* **2020**, *14*, 45–51. [CrossRef]
22. Zupanič, F.; Klemenc, J.; Steinacher, M.; Glodež, S. Microstructure, mechanical properties and fatigue behaviour of a new high-strength aluminium alloy AA 6086. *J. Alloys Compd.* **2023**, *941*, 168976. [CrossRef]
23. Yankin, A.S.; Mugatarov, A.I.; Wildemann, V.E. Influence of different loading paths on the multiaxial fatigue behavior of 2024 aluminum alloy under the same amplitude values of the second invariant of the stress deviator tensor. *Frat. Ed Integrita Strutt.* **2021**, *15*, 327–335. [CrossRef]
24. D'Angela, D.; Ercolino, M.; Bellini, C.; Di Cocco, V.; Iacoviello, F. Characterisation of the damaging micromechanisms in a pearlitic ductile cast iron and damage assessment by acoustic emission testing. *Fatigue Fract. Eng. Mater. Struct.* **2020**, *43*, 1038–1050. [CrossRef]
25. D'Angela, D.; Ercolino, M.; Bellini, C.; Di Cocco, V.; Iacoviello, F. Failure criteria for real-time assessment of ductile cast irons subjected to various loading conditions. *Smart Mater. Struct.* **2020**, *30*, 017001. [CrossRef]
26. Cui, Y.; Li, X.; Zhang, T.; Ding, W.; Yin, J. Development of High-Temperature Wire-Grid Thin Film Strain Gauges. *Sensors* **2022**, *22*, 7595. [CrossRef]
27. Kordell, J.; Yu, M.; Dasgupta, A. A fiber optic conjugate stress sensor for instantaneous tangent modulus detection targeting prognostic health monitoring applications. *Smart Mater. Struct.* **2022**, *31*, 075001. [CrossRef]

28. Brindisi, A.; Vendittozzi, C.; Travascio, L.; Di Palma, L.; Ignarra, M.; Fiorillo, V.; Concilio, A. Preliminary Assessment of an FBG-Based Landing Gear Weight on Wheel System. *Actuators* **2022**, *11*, 191. [CrossRef]
29. *ASTM D3166-99*; Standard Test Method for Fatigue Properties of Adhesive in Shear by Tension Loading (Metal/Metal). ASTM International: West Conshohocken, PA, USA, 2020. [CrossRef]